Vector-magnetic-field sensing via multifrequency control of nitrogen-vacancy centers in diamond

Sayaka Kitazawa,[1] Yuichiro Matsuzaki,[2] Soya Saijo,[1] Kosuke Kakuyanagi,[2] Shiro Saito,[2] and Junko Ishi-Hayase[1]

[1]*Department of Applied Physics and Department of Physico-Informatics, Faculty of Science and Technology, Keio University, Hiyoshi, Kohoku-ku, Yokohama 223-8522, Japan*

[2]*NTT Basic Research Laboratories, NTT Corporation, 3-1 Morinosato-Wakamiya, Atsugi, Kanagawa 243-0198, Japan*

(Received 3 May 2017; published 26 October 2017)

An ensemble of nitrogen-vacancy (NV) centers in diamond is an attractive device to detect small magnetic fields. In particular, by exploiting the fact that the NV center can be aligned along one of four different axes due to C_{3v} symmetry, it is possible to extract information concerning vector magnetic fields. However, in the conventional scheme, low readout contrasts of the NV centers significantly decrease the sensitivity of the vector-magnetic-field sensing. Here, we propose a way to improve the sensitivity of the vector-magnetic-field sensing of the NV centers using multifrequency control. Since the Zeeman energy of the NV centers depends on the direction of the axis, we can independently control the four types of NV centers using microwave pulses with different frequencies. This allows us to use every NV center for the vector field detection in parallel, which effectively increases the readout contrast. Our results pave the way to realize a practical diamond-based vector field sensor.

DOI: 10.1103/PhysRevA.96.042115

I. INTRODUCTION

The detection of small magnetic fields is important in the field of metrology, because there are many potential applications in biology and medical science. The performance of a magnetic field sensor is characterized by its spatial resolution and sensitivity; therefore, a significant amount of effort has been devoted to creating a device that can measure small magnetic fields in a local region [1–3].

Nitrogen-vacancy (NV) centers in diamond are fascinating candidates with which to construct a magnetic field sensor [4–7]. The NV center is a spin-1 system, and the frequency of the $|\pm1\rangle$ states can be shifted by magnetic fields. We can use this system as an effective two-level system spanned by $|0\rangle$ and $|1\rangle$ with a frequency selectivity where $|-1\rangle$ is significantly detuned. We can implement gate operations of the spins in NV centers using microwave pulses [8–11]. It is possible to detect dc (ac) magnetic fields by implementing a Ramsey interference (spin echo) measurement [4–6]. Moreover, NV centers have a long coherence time, e.g., a few milliseconds at a room temperature and a second at low temperature [12–14]. In addition, because the NV centers can be strongly coupled with optical photons, we can read out the state of the NV centers via fluorescence from the optical transitions [9,10]. The NV centers can be embedded in nanocrystals, which allows the NV centers to interact with local magnetic fields [15]. These properties are a prerequisite to realizing a high-performance sensor for magnetic fields.

Recently, vector-magnetic-field sensing by NV centers has become an active area of interest [16–21]. The NV center is aligned along one of four different axes due to C_{3v} symmetry. The Zeeman energies of the NV centers are determined by $g\mu_b\mathbf{B}\cdot\mathbf{d}_l$ $(l=1,2,3,4)$ where g denotes the g factor, μ_b denotes a Bohr magneton, $\mathbf{B}$ denotes the magnetic fields, and $\mathbf{d}_l$ denotes the direction of the lth NV axis. By sequentially performing Ramsey interference or spin echo measurements on NV centers with different NV axes, we can estimate the values of the Zeeman energies $g\mu_b\mathbf{B}\cdot\mathbf{d}_l$. The data from the experiments can be processed to reconstruct the vector components (B_x, B_y, and B_z) of applied magnetic fields [16,18]. This can be used to magnetically image a target sample such as living cells or circuit currents [22,23].

In the conventional approach, the low readout contrast of the NV centers decreases the sensitivity when sensing the vector magnetic field [5,24]. When the state of the NV centers is $|\pm1\rangle$, the photoluminescence intensity becomes smaller than in the case of $|0\rangle$. This allows us to measure the state of the NV centers via optical detection even at room temperature.

Nevertheless, we can only detect a small portion of the emitted photons, because most of the photons are emitted into the environment. This decreases the readout contrast. Moreover, if we only implement Ramsey or spin echo measurements on NV centers with a specific axis with this limited readout contrast, the states of the other NV centers with different axes remain in the $|0\rangle$ state regardless the value of the magnetic fields, which induces noise affecting the sensitivity of the magnetic field sensor [5]. If we only need to estimate one vector component of the target magnetic field, we can recover the sensitivity by using a diamond where the orientations of the NV centers are aligned along just one axis [25–28]. However, we cannot use such a diamond to estimate every component of the vector magnetic fields, unless we mechanically rotate the diamond to change the angle between the target magnetic fields and the direction of the NV axis.

Here, we propose a scheme to improve the sensitivity of the vector magnetic field sensing via multifrequency control. We consider using high-density NV centers in a bulk diamond where the NV centers have four different symmetry axes (Fig. 1). Because NV centers with different axes can have different resonant frequencies [24], we can independently control these NV centers via frequency selectivity. The key idea in our scheme is the simultaneous implementation of a Ramsey interference or spin echo experiment with every NV center via multifrequency control. We show that adequate control of the microwave pulses can enhance the signal from NV centers with four different axes, and that the sensitivity of the vector-magnetic-field sensing becomes approximately four times better than that of the conventional scheme.

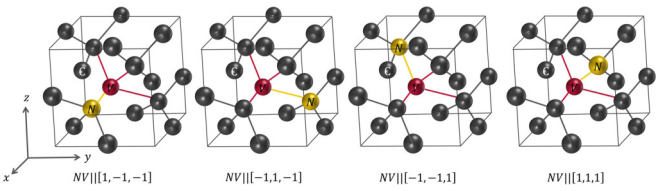

FIG. 1. An NV center in diamond set on an axis to be the direction from the vacancy to the nitrogen. There are four possible directions of the axis in the diamond. Note that by applying known external magnetic fields, we can independently control the four types of NV centers with different axes using frequency selectivity.

II. CONVENTIONAL VECTOR-MAGNETIC-FIELD SENSING WITH AN NV CENTER

Here, we review a conventional dc magnetic field sensing using NV centers [16–18]. The key idea in this scheme is to use NV centers with different axes so that we can extract the information of the vector magnetic fields. Applying microwave pulses to drive the states only with one specific NV axis, the photoluminescence intensity let us obtain the information of the magnetic field projection along the chosen NV axis. By repeating the experiment with different axes, we obtain the information of the magnetic field projection along different directions. From the sum of these experimental results, it is possible to extract the information of the vector magnetic fields. This scheme will, in principle, work for 4 NV centers with different axes. Although an ensemble of the NV centers is used for the actual experiment of the vector field sensing [16–18], we explain the case of using just four NV centers with different NV axes, which lets us know the essence of the conventional scheme.

We describe the details of the conventional dc magnetic field sensing using four NV centers with different axes. Even though the NV center is a spin-1 system, we can treat it as a two-level system spanned by $|0\rangle$ and $|1\rangle$ with frequency selectivity, as we show in detail in Appendix A. Note that the NV center has four types of intrinsic quantization axes along the NV direction with zero or small magnetic fields. We define the direction of these NV axes as $\mathbf{d}_1 = (\frac{1}{\sqrt{3}}, -\frac{1}{\sqrt{3}}, -\frac{1}{\sqrt{3}})$, $\mathbf{d}_2 = (-\frac{1}{\sqrt{3}}, \frac{1}{\sqrt{3}}, -\frac{1}{\sqrt{3}})$, $\mathbf{d}_3 = (-\frac{1}{\sqrt{3}}, -\frac{1}{\sqrt{3}}, \frac{1}{\sqrt{3}})$, and $\mathbf{d}_4 = (\frac{1}{\sqrt{3}}, \frac{1}{\sqrt{3}}, \frac{1}{\sqrt{3}})$.

The Hamiltonian of the NV center with an axis defined by a vector $\mathbf{d}_l$ is given as

$$H_l = \frac{\omega_l}{2}\hat{\sigma}_z^{(l)} + \lambda\hat{\sigma}_x^{(l)}\cos\omega' t, \tag{1}$$

for $l = 1,2,3,4$, where $\omega_l = \omega_0 + g\mu_b\mathbf{B}_{\text{total}}\cdot\mathbf{d}_l$, ω_0 denotes zero-field splitting, and $g\mu_b\mathbf{B}_{\text{total}}\cdot\mathbf{d}_l$ denotes Zeeman energy splitting.

$\mathbf{B}_{\text{total}} = \mathbf{B}_{\text{ex}} + \mathbf{B}$ denotes the sum of a known external magnetic field ($\mathbf{B}_{\text{ex}}$) and the target unknown magnetic field ($\mathbf{B}$), λ denotes the Rabi frequency, and ω' denotes the microwave frequency. The Pauli matrices are defined as $\hat{\sigma}_z = |1\rangle\langle 1| - |0\rangle\langle 0|, \hat{\sigma}_x = |1\rangle\langle 0| + |0\rangle\langle 1|, \hat{\sigma}_y = -i|1\rangle\langle 0| + i|0\rangle\langle 1|$. We consider $\hbar = 1$ here. Throughout this paper, we assume that the target unknown magnetic field ($\mathbf{B}$) is much smaller than the known external magnetic field ($\mathbf{B}_{\text{ex}}$). By applying known external magnetic fields of around 5 mT, the degeneracy of the four different orientations of NV centers can be removed,

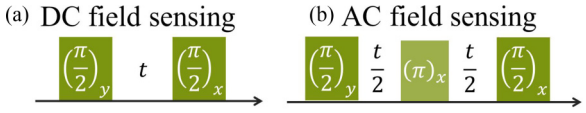

FIG. 2. Microwave pulse sequence for standard magnetometry with NV centers. (a) Ramsey interference measurements performed to sense dc field, and (b) spin echo measurements performed to sense the ac field where we can suppress low-frequency magnetic field noise.

and so the resonant frequency of the NV centers is different depending on the NV axis [24]. We can drive only the NV centers with an axis $\mathbf{d}_k$ by resonant microwave pulses where k denotes the specific NV center to be driven by the microwave, while the other NV centers with different axes are not driven by the microwave pulses because of the energy detuning. Also, we assume that the Zeeman energy due to the external magnetic fields ($g\mu_b\mathbf{B}_{\text{ex}}\cdot\mathbf{d}_l$ for $l = 1,2,3,4$) is much smaller than the zero-field splitting of the NV centers (ω_0). This guarantees that the eigenstates of the Hamiltonian are $|0\rangle$ and $|1\rangle$ without microwave driving.

In a rotating frame, we can rewrite this Hamiltonian as

$$H_l = \frac{\omega_l - \omega'}{2}\hat{\sigma}_z^{(l)} + \frac{\lambda}{2}\hat{\sigma}_x^{(l)}, \tag{2}$$

for $l = 1,2,3,4$, where we choose $\omega' = \omega_0 + g\mu_b\mathbf{B}_{\text{ex}}\cdot\mathbf{d}_k$ and use a rotating-wave approximation. Due to a large detuning, we obtain

$$H_{k'} \simeq \frac{g\mu_b\mathbf{B}_{\text{total}}\cdot\mathbf{d}_{k'} - g\mu_b\mathbf{B}_{\text{ex}}\cdot\mathbf{d}_k}{2}\hat{\sigma}_z^{(k')}, \tag{3}$$

for $k' \neq k$, where k' denote the NV centers not to be driven by the microwave. On the other hand, since we assume $g\mu_b\mathbf{B}\cdot\mathbf{d}_k \ll \lambda$, we have

$$H_k \simeq \frac{\lambda}{2}\hat{\sigma}_x^{(k)} \tag{4}$$

during the application of the microwave pulses. If we do not apply a microwave ($\lambda = 0$), the Hamiltonian is written as

$$H_l = \frac{g\mu_b\mathbf{B}_{\text{total}}\cdot\mathbf{d}_l - g\mu_b\mathbf{B}_{\text{ex}}\cdot\mathbf{d}_k}{2}\hat{\sigma}_z^{(l)}, \tag{5}$$

for $l = 1,2,3,4$. We can construct the vector field sensor as follows [see Fig. 2(a)]. We assume that the initialization time, pulse operations, and readout time are much shorter than the coherence time of the NV center. First, we initialize the state to obtain $\bigotimes_{l=1}^{4}|0\rangle_l$ via green laser irradiation. Second, by performing a $\frac{\pi}{2}$ pulse along the y axis with the microwave (resonant on the kth NV center), we prepare $|+\rangle_k\bigotimes_{k'\neq k}|0\rangle_{k'}$ where $|+\rangle_k = \frac{1}{\sqrt{2}}(|0\rangle_k + |1\rangle_k)$ state. Third, we let this state evolve via the Hamiltonian in Eq. (5) for a time t_k. Note that the NV center is affected by the dephasing process; therefore, the dynamics can be described by the following master equation:

$$\frac{d\rho_l}{dt} = -i[H_l,\rho_l] - \gamma_l\left(\rho_l - \hat{\sigma}_z^{(l)}\rho_l\hat{\sigma}_z^{(l)}\right), \tag{6}$$

where $\gamma_l = \frac{1}{2T_2^{l*}}$ denotes the dephasing rate of the lth NV center and T_2^{l*} denotes the coherence time measured by Ramsey interference for $l = 1,2,3,4$. It is worth mentioning that, since

the energy relaxation rate is usually much smaller than the dephasing rate in the NV centers [29], we ignore the energy relaxation throughout of this paper. In this case, if we prepare an energy eigenstate such as $|0\rangle$ or $|1\rangle$, such a state does not change during a time scale that we are interested in. So, during this process, the NV centers with an axis of $\mathbf{d}_{k'}$ ($k' \neq k$) remain in a state of $\bigotimes_{k'\neq k}|0\rangle_{k'}$. Fourth, we perform a $\frac{\pi}{2}$ pulse along the x axis with the microwave (resonant on the kth NV center). The diagonal component of the density matrix after these operations can be calculated to be

$$ {}_k\langle 0|\rho_k(t_k)|0\rangle_k = \frac{1+e^{-2\gamma_k t_k}\sin(g\mu_b\mathbf{B}\cdot\mathbf{d}_k t_k)}{2}, \tag{7}$$

$$ {}_k\langle 1|\rho_k(t_k)|1\rangle_k = \frac{1-e^{-2\gamma_k t_k}\sin(g\mu_b\mathbf{B}\cdot\mathbf{d}_k t_k)}{2}, \tag{8}$$

while the diagonal components of the density matrices for the other NV centers with an axis of $\mathbf{d}_{k'}$ are ${}_{k'}\langle 0|\rho_{k'}(t_k)|0\rangle_{k'} = 1$ and ${}_{k'}\langle 1|\rho_{k'}(t_k)|1\rangle_{k'} = 0$ for $k' \neq k$ due to the detuning. Finally, we readout the population of the state via the green laser irradiation [9]. The information of the NV center is now transferred into photons, and the photon state is described as

$$\begin{aligned}\rho^{(\mathrm{ph})} = \Bigg[&\frac{1+e^{-2\gamma_k t_k}\sin(g\mu_b\mathbf{B}\cdot\mathbf{d}_k t_k)}{2}\rho_{k,0}^{(\mathrm{ph})} \\ &+ \frac{1-e^{-2\gamma_k t_k}\sin(g\mu_b\mathbf{B}\cdot\mathbf{d}_k t_k)}{2}\rho_{k,1}^{(\mathrm{ph})}\Bigg]\bigotimes_{k'\neq k}\rho_{k',0}^{(\mathrm{ph})},\end{aligned} \tag{9}$$

where $\rho_{l,1}^{(\mathrm{ph})}$ ($\rho_{l,0}^{(\mathrm{ph})}$) denotes the state of the photon after performing the green laser pulse when the state of the NV center is $|1\rangle_l$ ($|0\rangle_l$) for $l = 1,2,3,4$. We can describe $\rho_{l,1}^{(\mathrm{ph})}$ and $\rho_{l,0}^{(\mathrm{ph})}$ as follows:

$$\begin{aligned}\rho_{l,0}^{(\mathrm{ph})} &= \left(1-\alpha_0^{(l)}\right)|0\rangle_{\mathrm{ph}}\langle 0| + \alpha_0^{(l)}|1\rangle_{\mathrm{ph}}\langle 1|, \\ \rho_{l,1}^{(\mathrm{ph})} &= \left(1-\alpha_1^{(l)}\right)|0\rangle_{\mathrm{ph}}\langle 0| + \alpha_1^{(l)}|1\rangle_{\mathrm{ph}}\langle 1|,\end{aligned}$$

where $|0\rangle_{\mathrm{ph}}$ and $|1\rangle_{\mathrm{ph}}$ denote the Fock states of the photon. We define $\alpha_0^{(l)}$ ($\alpha_1^{(l)}$) $l = 1,2,3,4$ as a probability emitting a photon when the state of the NV center is $|0\rangle_l$ ($|1\rangle_l$). Note that while we control the NV center with the NV axis along $\mathbf{d}_k$, the other NV centers remain in the state of $|0\rangle_{k'}$ ($k' \neq k$) and emit photons. We assume $\alpha_0^{(l)}, \alpha_1^{(l)} \ll 1$ and that the multiple photon emission probability from an NV center is negligible. We define a photon number operator as $\hat{N} = \sum_{l=1}^{4}\hat{a}_l^\dagger\hat{a}_l$ where $\hat{a}_l^\dagger$ ($\hat{a}_l$) denotes the creation (destruction) operator of the photon emitted from the NV center with an NV axis of $\mathbf{d}_\mathbf{l}$. For $g\mu_b\mathbf{B}\cdot\mathbf{d}_k t_k \ll 1$, we can calculate the expectation value of the emitted photons

$$\begin{aligned}\langle\hat{N}_k\rangle &= \mathrm{Tr}[\rho^{(\mathrm{ph})}\hat{N}] \\ &\simeq \frac{1+g\mu_b\mathbf{B}\cdot\mathbf{d}_k t_k e^{-2\gamma_k t_k}}{2}\tilde{\alpha}_0 \\ &+ \frac{1-g\mu_b\mathbf{B}\cdot\mathbf{d}_k t_k e^{-2\gamma_k t_k}}{2}\tilde{\alpha}_1^{(k)},\end{aligned} \tag{10}$$

where we define $\tilde{\alpha}_0 = \sum_{l=1}^{4}\alpha_0^{(l)}$ and $\tilde{\alpha}_1^{(k)} = \alpha_1^{(k)} + \sum_{k'\neq k}\alpha_0^{(k')}$. Note that we can tune $\alpha_0^{(l)}$ and $\alpha_1^{(l)}$ by changing both light field amplitudes and the polarization of the photons. In addition, we can decrease the coherence time if we add artificial noise. For simplicity, we assume $\alpha_0^{(l)} = \alpha_0$, $\alpha_1^{(l)} = \alpha_1$, $\gamma_l = \gamma$, and $t_l = t$ for ($l = 1,2,3,4$). Suppose that we first implement the above experiment shown in Fig. 2(a) for $k = 1$, and then implement it for $k = 4$, which allows us to sum up these two experimental data, and we obtain

$$\langle\hat{N}_1\rangle + \langle\hat{N}_4\rangle = (\tilde{\alpha}_0+\tilde{\alpha}_1) + \frac{1}{\sqrt{3}}(\tilde{\alpha}_0-\tilde{\alpha}_1)g\mu_b B_x t e^{-2\gamma t}. \tag{11}$$

Interestingly, this sum depends on B_x while this is independent of B_y and B_z. Therefore we define $\langle\hat{N}_x\rangle \equiv \langle\hat{N}_1\rangle + \langle\hat{N}_4\rangle$, and we estimate B_x from $\langle\hat{N}_x\rangle$. Note that even though we explain the case to measure B_x, we can also measure B_y (B_z) by considering $\langle\hat{N}_y\rangle \equiv \langle\hat{N}_2\rangle + \langle\hat{N}_4\rangle$ ($\langle\hat{N}_z\rangle \equiv \langle\hat{N}_3\rangle + \langle\hat{N}_4\rangle$), because $\langle\hat{N}_y\rangle$ ($\langle\hat{N}_z\rangle$) only depends on B_y (B_z). Therefore, we can calculate the uncertainty in the estimation of B_x as follows:

$$\begin{aligned}\delta B_x^{(\mathrm{dc})} &= \frac{\sqrt{\langle\delta\hat{N}_x\delta\hat{N}_x\rangle}}{\left|\frac{d\langle\hat{N}\rangle_x}{dB_x}\right|}\frac{1}{\sqrt{N}} \\ &= \frac{\sqrt{3}\sqrt{7\alpha_0+\alpha_1}}{|\alpha_0-\alpha_1|g\mu_b t e^{-2\gamma t}}\frac{1}{\sqrt{\frac{T}{2t}}},\end{aligned} \tag{12}$$

where $N = \frac{T}{2t}$ denotes the repetition number and T denotes the total experiment time. This uncertainty is minimized for $t = \frac{1}{4\gamma}$ and

$$\delta B_x^{(\mathrm{dc})} = \frac{\sqrt{3}\sqrt{7\alpha_0+\alpha_1}}{e^{-\frac{1}{4}}|\alpha_0-\alpha_1|g\mu_b\sqrt{\frac{1}{4\gamma}}}\frac{1}{\sqrt{\frac{T}{2}}}. \tag{13}$$

Therefore we chose this value for the field sensing. Note that we have a factor of $\sqrt{7\alpha_0+\alpha_1}$ in the numerator, which increases the uncertainty. This is because, when we read out the NV centers, three-quarters of the NV centers remain in the $|0\rangle$ state regardless of the strength of the magnetic fields, which decreases the sensitivity. This clearly shows that the existence of NV centers that emit the same number of photons regardless of the strength of the applied magnetic field actually decreases the sensitivity of the field sensing.

Here, we briefly review conventional ac magnetic field sensing using NV centers [5,16,17]. We have the same form of the Hamiltonian described in Eq. (B1) where we replace the total magnetic field with $\mathbf{B}_{\mathrm{total}} = \mathbf{B}_{\mathrm{ex}} + \mathbf{B}_{\mathrm{ac}}\sin\omega_{\mathrm{ac}}t$. Here, we assume that we can control ω_{ac} while $\mathbf{B}_{\mathrm{ac}}$ is unknown. This is a reasonable assumption when we try to detect nuclear spins, because we can rotate the spin by radio frequency pulses while we do not know the states of the nuclear spin [30]. This assumption is also valid when we try to detect a state of the superconducting flux qubit [31]. The superconducting flux qubit has two persistent current states, and we can measure the superconducting flux qubit by detecting the magnetic field from the flux qubit. To induce ac magnetic fields with a controllable frequency of ω_{ac}, we can drive the flux qubit by a resonant pulse [32].

To estimate the values of $\mathbf{B}_{\mathrm{ac}}$, we use a similar pulse sequence to that of the dc magnetic field sensing. The only difference from the dc magnetic field sensing is that we apply

a π pulse in the middle of the time evolution between the two $\frac{\pi}{2}$ pulses, as shown in Fig. 2(b). The diagonal component of the density matrix can be calculated as

$$ {}_k\langle 0|\rho_k(t_k)|0\rangle_k = \frac{1+e^{-2\gamma_k' t_k}\sin\theta_k^{(\mathrm{ac})}}{2}, \tag{14}$$

$$ {}_k\langle 1|\rho_k(t_k)|1\rangle_k = \frac{1-e^{-2\gamma_k' t_k}\sin\theta_k^{(\mathrm{ac})}}{2}, \tag{15}$$

$$ \theta_k^{(\mathrm{ac})} = g\mu_b \mathbf{B}_{\mathrm{ac}}\cdot\mathbf{d}_k \frac{1+\cos\omega_{\mathrm{ac}}t-2\cos\frac{\omega_{\mathrm{ac}}t}{2}}{\omega_{\mathrm{ac}}}, \tag{16}$$

where $\gamma_k' = \frac{1}{2T_2^k}$ denotes the dephasing rate for the k'th NV center and T_2^k denotes the dephasing time measured by the spin echo. The diagonal components of the density matrices for the other NV centers with an axis of $\mathbf{d}_{k'}$ $(k' \neq k)$ are ${}_{k'}\langle 0|\rho_{k'}(t_k)|0\rangle_{k'} = 1$ and ${}_{k'}\langle 1|\rho_{k'}(t_k)|1\rangle_{k'} = 0$ for $k' \neq k$ due to the detuning. Similarly to the case of dc sensing, we can calculate the sensitivity of the ac field sensing such that

$$ \delta B_x^{(\mathrm{ac})} \simeq \frac{\sqrt{3}\sqrt{7\alpha_0+\alpha_1}}{|\alpha_0-\alpha_1|g\mu_b\frac{|1+\cos\omega_{\mathrm{ac}}t-2\cos\frac{\omega_{\mathrm{ac}}t}{2}|}{\omega_{\mathrm{ac}}}e^{-2\gamma' t}}\frac{1}{\sqrt{\frac{T}{2t}}}, \tag{17}$$

where we assume $\alpha_0^{(k)} = \alpha_0$, $\alpha_1^{(k)} = \alpha_1$, $\gamma_k' = \gamma'$, and $t_k = t$ for all k. This uncertainty is minimized for $t = \frac{1}{4\gamma'}$ and $\omega_{\mathrm{ac}} \simeq 23.3\gamma' = \frac{2\theta_{\mathrm{opt}}}{T_2}$ for $\theta_{\mathrm{opt}} \simeq 1.856\pi$. So we choose these values for the field sensing. The uncertainty in the estimation is given as follows:

$$ \delta B_x^{(\mathrm{ac})} \simeq \frac{\sqrt{3}\sqrt{7\alpha_0+\alpha_1}}{e^{-\frac{1}{2}}|\alpha_0-\alpha_1|g\mu_b\frac{|1+\cos\theta_{\mathrm{opt}}-2\cos\frac{\theta_{\mathrm{opt}}}{2}|}{\theta_{\mathrm{opt}}}\sqrt{\frac{1}{4\gamma'}\frac{T}{2}}}. \tag{18}$$

III. DC-VECTOR-MAGNETIC-FIELD SENSOR VIA MULTIFREQUENCY CONTROL

Here, we propose a scheme to measure the vector magnetic field with an improved sensitivity. The key idea is to adopt multifrequency control of the NV centers. NV centers with different axes can have different resonant frequencies when applying a known external magnetic field [24]; therefore, we can independently control these NV centers using frequency selectivity. In addition, we can parallelize the control of the NV centers by simultaneously rotating all NV centers with different axes so that every NV center can be involved in the field sensing.

It is worth mentioning that to demonstrate our proposal, we can use a large ensemble of NV centers where each NV center has different properties, as we will describe later. However, for simplicity, we start by explaining how our scheme works if we have four specific NV centers with the NV axis of $\mathbf{d}_1$, $\mathbf{d}_2$, $\mathbf{d}_3$, and $\mathbf{d}_4$ where the NV centers have the same properties except the NV axis.

We consider detecting a weak target unknown magnetic field ($\mathbf{B}$) along the general direction by using our scheme. As an example, we explain how to measure a dc magnetic field component along [1,0,0] (B_x) using our scheme. After the initialization of the states by the green laser, we rotate every NV center using the $\frac{\pi}{2}$ pulse, and the initial state is given by $\bigotimes_{l=1}^4 \frac{1}{\sqrt{2}}(|0\rangle_l + |1\rangle_l)$. Although we assume a perfect single-qubit gate here, we will describe the effect of the imperfect single-qubit gate in Appendixes B and C. We let this state evolve for a time t according to the master equation in Eq. (C5). After performing the $\frac{\pi}{2}$ pulse ($\frac{3\pi}{2}$ pulse) on the NV centers with the NV axes $\mathbf{d}_2$ and $\mathbf{d}_3$ ($\mathbf{d}_1$ and $\mathbf{d}_4$) as shown in Fig. 3(a), we read out the state of the NV centers via the photoluminescence. The diagonal component of the density matrix just before the readout can be calculated as

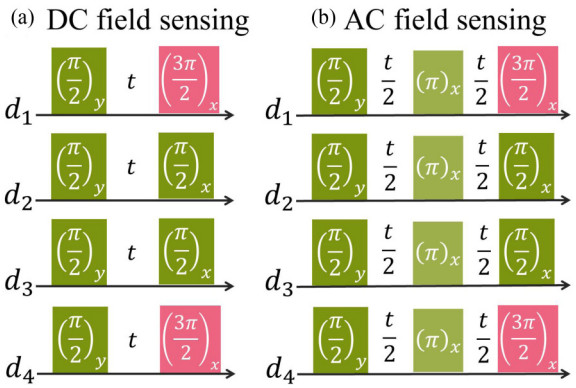

FIG. 3. The pulse sequence used to perform our proposed vector-magnetic-field sensing. Using frequency selectivity, we independently control the NV centers with different axes. We implement four microwave pulses with different frequencies at the same time to increase the sensitivity.

$$ {}_k\langle 0|\rho_k(t_k)|0\rangle_k = \frac{1+e^{-2\gamma_k t_k}\sin(g\mu_b\mathbf{B}\cdot\mathbf{d}_k t_k)}{2},$$
$$ {}_k\langle 1|\rho_k(t_k)|1\rangle_k = \frac{1-e^{-2\gamma_k t_k}\sin(g\mu_b\mathbf{B}\cdot\mathbf{d}_k t_k)}{2}, \tag{19}$$

for $k = 2,3$ and

$$ {}_k\langle 0|\rho_k(t_k)|0\rangle_k = \frac{1-e^{-2\gamma_k t_k}\sin(g\mu_b\mathbf{B}\cdot\mathbf{d}_k t_k)}{2},$$
$$ {}_k\langle 1|\rho_k(t_k)|1\rangle_k = \frac{1+e^{-2\gamma_k t_k}\sin(g\mu_b\mathbf{B}\cdot\mathbf{d}_k t_k)}{2}, \tag{20}$$

for $k = 1,4$. After the green laser irradiation, the state of the photons can be described as $\rho^{(\mathrm{ph})} = \bigotimes_{l=1}^4 \rho_l^{(\mathrm{ph})}$, where

$$ \rho_k^{(\mathrm{ph})} = \frac{1+e^{-2\gamma_k t_k}\sin(g\mu_b\mathbf{B}\cdot\mathbf{d}_k t_k)}{2}\rho_{k,0}^{(\mathrm{ph})} + \frac{1-e^{-2\gamma_k t_k}\sin(g\mu_b\mathbf{B}\cdot\mathbf{d}_k t_k)}{2}\rho_{k,1}^{(\mathrm{ph})}, \tag{21}$$

for $k = 2,3$ and

$$ \rho_k^{(\mathrm{ph})} = \frac{1-e^{-2\gamma_k t_k}\sin(g\mu_b\mathbf{B}\cdot\mathbf{d}_k t_k)}{2}\rho_{k,0}^{(\mathrm{ph})} + \frac{1+e^{-2\gamma_k t_k}\sin(g\mu_b\mathbf{B}\cdot\mathbf{d}_k t_k)}{2}\rho_{k,1}^{(\mathrm{ph})}, \tag{22}$$

for $k = 1,4$. We can calculate the expected values of the emitted photons from these states as follows:

$$\begin{aligned}\langle \hat{N}_x^{(\mathrm{total})} \rangle &= \mathrm{Tr}\left[\left(\sum_{l=1}^{4} \hat{N}_k\right)\rho^{(\mathrm{ph})}\right] \\ &\simeq \sum_{l=1}^{4} \frac{\alpha_0^{(l)} + \alpha_1^{(l)}}{2} \\ &\quad - \sum_{k=1,4} \frac{\alpha_0^{(k)} - \alpha_1^{(k)}}{2} g\mu_b \mathbf{B}\cdot\mathbf{d}_k t_k e^{-2\gamma_k t_k} \\ &\quad + \sum_{k=2,3} \frac{\alpha_0^{(k)} - \alpha_1^{(k)}}{2} g\mu_b \mathbf{B}\cdot\mathbf{d}_k t_k e^{-2\gamma_k t_k}. \end{aligned} \tag{23}$$

Let us assume $\alpha_0^{(l)} = \alpha_0$, $\alpha_1^{(l)} = \alpha_1$, $\gamma_l = \gamma$, and $t_l = t$ ($l = 1,2,3,4$) for simplicity. (We will consider more general conditions later.) With these homogeneous parameters, we obtain

$$\langle \hat{N}_x^{(\mathrm{total})} \rangle \simeq 2(\alpha_0 + \alpha_1) - \frac{2}{\sqrt{3}}(\alpha_0 - \alpha_1) g\mu_b B_x t e^{-2\gamma t}.$$

Note that this expectation value depends on just B_x. Therefore, the uncertainty of the estimation of B_x is given as follows:

$$\begin{aligned}\delta B_x^{(\mathrm{dc})} &= \frac{\sqrt{\langle \delta\hat{N}_x^{(\mathrm{total})} \delta\hat{N}_x^{(\mathrm{total})} \rangle}}{\left|\frac{d\langle \hat{N}_x^{(\mathrm{total})}\rangle}{dB_x}\right|} \frac{1}{\sqrt{N}} \\ &\simeq \frac{\sqrt{2(\alpha_0+\alpha_1)}}{\frac{2}{\sqrt{3}}|\alpha_0 - \alpha_1| g\mu_b t e^{-2\gamma t}} \frac{1}{\sqrt{\frac{T}{t}}}, \end{aligned} \tag{24}$$

where $N = \frac{T}{t}$ denotes the repetition number of the experiment. This uncertainty is minimized for $t = \frac{1}{4\gamma}$ and

$$\delta B_x^{(\mathrm{dc})} \simeq \frac{\sqrt{3}\sqrt{2(\alpha_0+\alpha_1)}}{2e^{-\frac{1}{2}}|\alpha_0 - \alpha_1| g\mu_b \sqrt{\frac{1}{4\gamma}}} \frac{1}{\sqrt{T}}. \tag{25}$$

Therefore, we chose this value for the field sensing. Because we have $\alpha_0 \simeq \alpha_1$ due to the low readout contrast [24], the sensitivity of our scheme described by Eq. (25) is approximately four times better than that in the conventional scheme described by Eq. (13). Note that even though we explained how to measure the magnetic field B_x along [1,0,0], we can easily generalize our scheme to measure B_y and B_z. For example, to measure B_y (B_z), we perform a $\frac{\pi}{2}$ pulse ($\frac{3\pi}{2}$ pulse) on the NV centers with the NV axes of $\mathbf{d}_1$ and $\mathbf{d}_3$ ($\mathbf{d}_2$ and $\mathbf{d}_4$) between the green laser irradiation.

However, in actual experiments, $\alpha_0^{(l)}$, $\alpha_1^{(l)}$, and γ_l have a dependency on l due to inhomogeneities. In this case, we need to choose a suitable set of t_l ($l = 1,2,3,4$) to compensate for such an inhomogeneity. If $\tau_l(t_l) \equiv \frac{\alpha_0^{(l)} - \alpha_1^{(l)}}{2} e^{-2\gamma_l t_l} t_l$ does not depend on l, we can measure B_x from $\langle \hat{N}_x^{(\mathrm{total})} \rangle$ as described in Eq. (23). We numerically checked that it is possible to have an equal value of $\frac{\alpha_0^{(l)} - \alpha_1^{(l)}}{2} e^{-2\gamma_l t_l} t_l$ for $l = 1,2,3,4$. In Fig. 4, we randomly picked up $\delta\alpha_j = \alpha_0^{(j)} - \alpha_1^{(j)}$ and γ_j from the Gaussian distribution, and we plotted $\tau_j(t) = \frac{\alpha_0^{(j)} - \alpha_1^{(j)}}{2} e^{-2\gamma_j t} t$ ($j = 1,2,\ldots,200$). (It is worth mentioning that although we still consider using four NV centers for our scheme, we choose 200 sets of random parameters to investigate the effect of inhomogeneous parameters between these four NV centers.) In addition, in the same figure, we plotted the value of $\frac{\delta\alpha_{\min}}{2} e^{-\frac{1}{2}} \frac{1}{4\gamma_{\max}}$ with a dashed line where $\delta\alpha_{\min} = \min_j[\delta\alpha_j]$ and $\gamma_{\max} = \max_j[\gamma_j]$. These results show that we can choose t_j to satisfy $\frac{\alpha_0^{(j)} - \alpha_1^{(j)}}{2} e^{-2\gamma_j t_j} t_j = \frac{\delta\alpha_{\min}}{2} e^{-\frac{1}{2}} \frac{1}{4\gamma_{\max}}$ and $t_j \leqslant \frac{1}{4\gamma_{\max}}$ as long as the inhomogeneous width of the parameters is approximately 10% [24]. The expected values of the emitted photons from this state are described as

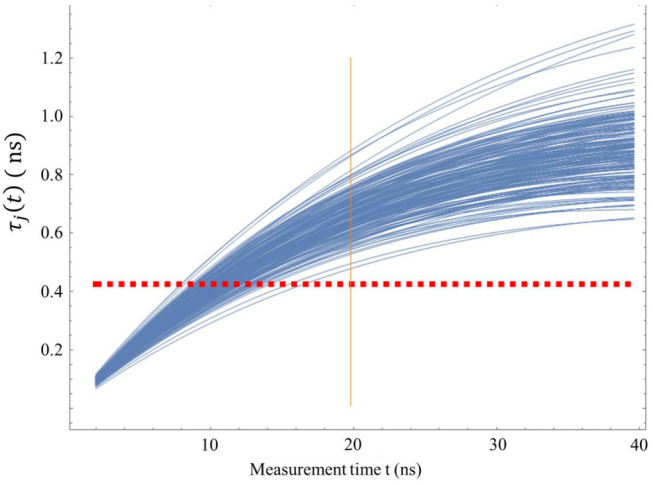

FIG. 4. We plot $\tau_j(t) = \frac{\alpha_0^{(j)} - \alpha_1^{(j)}}{2} e^{-2\gamma_j t} t$ ($j = 1,2,\ldots,200$) against t where we choose $\delta\alpha_j = \alpha_0^{(j)} - \alpha_1^{(j)}$ and γ_j from the Gaussian distribution. The average of $\delta\alpha_j$ (γ_j) is 0.01 (10^7 Hz), and the standard deviation is 0.001 (10^6). In addition, we plot the value of $\frac{\delta\alpha_{\min}}{2} e^{-\frac{1}{2}} \frac{1}{4\gamma_{\max}}$ with a horizontal dashed line, where $\delta\alpha_{\min} = \min_j[\delta\alpha_j]$ and $\gamma_{\max} = \max_j[\gamma_j]$, and plot a vertical line at $t = \frac{1}{4\gamma_{\max}}$. We numerically show that we can satisfy $\tau_j(t_j) = \frac{\delta\alpha_{\min}}{2} e^{-\frac{1}{2}} \frac{1}{4\gamma_{\max}}$ for all j by choosing a certain set of $\{t_j\}_{j=1}^{200}$ for $t_j \leqslant \frac{1}{4\gamma_{\max}}$.

$$\begin{aligned}\langle \hat{N}_x^{(\mathrm{total})} \rangle &\simeq \sum_{l=1}^{4} \frac{\alpha_0^{(l)} + \alpha_1^{(l)}}{2} \\ &\quad - \sum_{k=1,4} \frac{\alpha_0^{(k)} - \alpha_1^{(k)}}{2} g\mu_b \mathbf{B}\cdot\mathbf{d}_k t_k e^{-2\gamma_k t_k} \\ &\quad + \sum_{k=2,3} \frac{\alpha_0^{(k)} - \alpha_1^{(k)}}{2} g\mu_b \mathbf{B}\cdot\mathbf{d}_k t_k e^{-2\gamma_k t_k} \\ &= \left(\sum_{l=1}^{4} \frac{\alpha_0^{(l)} + \alpha_1^{(l)}}{2}\right) + \frac{2e^{-\frac{1}{2}}}{\sqrt{3}} \frac{\delta\alpha_{\min}}{4\gamma_{\max}} g\mu_b B_x, \end{aligned}$$

where $\delta\alpha_{\min} = \min_{l=1,2,3,4}[\alpha_0^{(l)} - \alpha_1^{(l)}]$ and $\gamma_{\max} = \max_{l=1,2,3,4}[\gamma_l]$.

Therefore, the uncertainty in the estimation of B_x is given as follows:

$$\begin{aligned}\delta B_x^{(\mathrm{dc})} &= \frac{\sqrt{\langle \delta\hat{N}_x^{(\mathrm{total})} \delta\hat{N}_x^{(\mathrm{total})} \rangle}}{\left|\frac{d\langle \hat{N}_x^{(\mathrm{total})}\rangle}{dB_x}\right|} \frac{1}{\sqrt{N}} \\ &\simeq \frac{\sqrt{3}\sqrt{\sum_{l=1}^{4} \frac{\alpha_0^{(l)} + \alpha_1^{(l)}}{2}}}{2e^{-\frac{1}{2}} \delta\alpha_{\min} g\mu_b \sqrt{\frac{1}{4\gamma_{\max}}}} \frac{1}{\sqrt{T}}. \end{aligned} \tag{26}$$

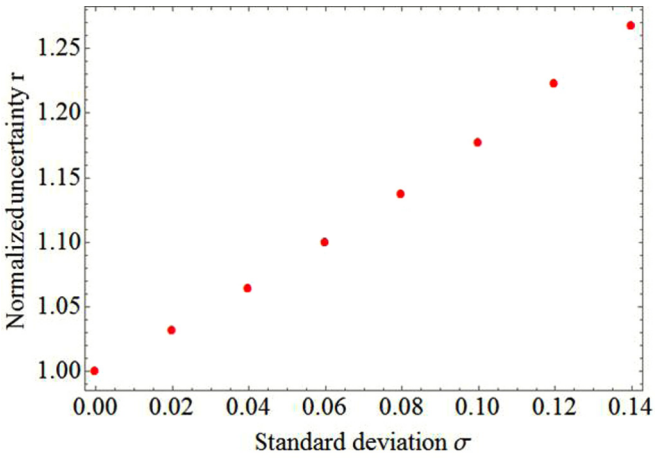

FIG. 5. The normalized uncertainty of the estimation $r = \delta B_x^{(\mathrm{dc})}(\sigma)/\delta B_x^{(\mathrm{dc})}(\sigma=0) = \delta B_x^{(\mathrm{ac})}(\sigma)/\delta B_x^{(\mathrm{ac})}(\sigma=0)$ where $\delta B_x^{(\mathrm{dc})}(\sigma)$ [$\delta B_x^{(\mathrm{ac})}(\sigma)$] denotes the uncertainty in our dc (ac) vector magnetic field sensor for inhomogeneous parameters with a standard deviation of σ. Note that the normalized uncertainty for the dc sensing has the same form as that for the ac sensing. To calculate the average value, we randomly pick up the values of $\delta\alpha_j = \alpha_0^{(j)} - \alpha_1^{(j)}$ and γ_j from the Gaussian distribution where the average of $\delta\alpha_j$ (γ_j) is $\overline{\delta\alpha_j} = 0.01$ ($\overline{\gamma_j} = 10^6$ Hz) and the standard deviation is $\overline{\delta\alpha_j}\cdot\sigma'$ ($\overline{\gamma_j'}\cdot\sigma'$) where σ' denotes a normalized standard deviation.

We numerically calculated this sensitivity, and plotted the ratio between the homogeneous case and inhomogeneous case with a standard deviation of σ as shown in Fig. 5. These results demonstrate that if the standard deviation of the parameters is around a few %, we can achieve nearly the same sensitivity as that in the homogeneous case.

We will consider a more realistic case where we use an ensemble of NV centers with slightly different properties, while we described the case of using four NV centers above. Similarly to the standard electron spin resonance (ESR), we will globally drive the NV centers by the microwave pulses where we use the same pulse sequence as shown in Fig. 3. After the initialization of the states by the green laser, we rotate the ensemble of NV centers by using the $\frac{\pi}{2}$ pulse, and the initial state is given by

$$\bigotimes_{j=1}^{\frac{L}{4}}\left[\bigotimes_{l=1}^{4}\frac{1}{\sqrt{2}}(|0\rangle_{l,j}+|1\rangle_{l,j})\right], \tag{27}$$

where L denotes the number of NV centers and l specifies the type of the NV axis. We can calculate the expected values of the emitted photons from the NV centers after the readout by the green laser as follows:

$$\begin{aligned}\langle\hat{N}_x^{(\mathrm{total})}\rangle \simeq& \sum_{j=1}^{\frac{L}{4}}\sum_{l=1}^{4}\frac{\alpha_0^{(l,j)}+\alpha_1^{(l,j)}}{2}\\ &-\sum_{j=1}^{\frac{L}{4}}\sum_{k=1,4}\frac{\alpha_0^{(k,j)}-\alpha_1^{(k,j)}}{2}g\mu_b\mathbf{B}\cdot\mathbf{d}_k t_k e^{-2\gamma_{k,j}t_k}\\ &+\sum_{j=1}^{\frac{L}{4}}\sum_{k=2,3}\frac{\alpha_0^{(k,j)}-\alpha_1^{(k,j)}}{2}g\mu_b\mathbf{B}\cdot\mathbf{d}_k t_k e^{-2\gamma_{k,j}t_k}.\end{aligned} \tag{28}$$

For $l = 1,2,3,4$, we define the deviation from the average value as $\delta\alpha_0^{(l,j)} \equiv \alpha_0^{(l,j)} - \alpha_0^{(l)}$, $\delta\alpha_1^{(l,j)} \equiv \alpha_1^{(l,j)} - \alpha_1^{(l)}$, and $\delta\gamma_{l,j} = \gamma_{l,j} - \gamma_l$ where $\alpha_0^{(l)}$ ($\alpha_1^{(l)}$) denotes an average value for $\{\alpha_0^{(l,j)}\}_{j=1}^{\frac{L}{4}}$ ($\{\alpha_1^{(l,j)}\}_{j=1}^{\frac{L}{4}}$) and γ_l denotes an average value for $\{\gamma_{l,j}\}_{j=1}^{\frac{L}{4}}$. We can rewrite the expectation value as $\langle\hat{N}_x^{(\mathrm{total})}\rangle = N_x^{(\mathrm{av})} + \delta N_x^{(\mathrm{av})}$. Here, $N_x^{(\mathrm{av})}$ denotes the average value defined as

$$\begin{aligned}N_x^{(\mathrm{av})} =& \frac{L}{4}\sum_{l=1}^{4}\frac{\alpha_0^{(l)}+\alpha_1^{(l)}}{2}\\ &-\frac{L}{4}\sum_{k=1,4}\frac{\alpha_0^{(k)}-\alpha_1^{(k)}}{2}g\mu_b\mathbf{B}\cdot\mathbf{d}_k t_k e^{-2\gamma_k t_k}\\ &+\frac{L}{4}\sum_{k=2,3}\frac{\alpha_0^{(k)}-\alpha_1^{(k)}}{2}g\mu_b\mathbf{B}\cdot\mathbf{d}_k t_k e^{-2\gamma_k t_k},\end{aligned}$$

while $\delta N_x^{(\mathrm{av})}$ denotes the deviation from the average values calculated as

$$\begin{aligned}\delta N_x^{(\mathrm{av})} \simeq& \sum_{j=1}^{\frac{L}{4}}\sum_{l=1}^{4}\frac{\delta\alpha_0^{(l,j)}+\delta\alpha_1^{(l,j)}}{2}\\ &-\sum_{j=1}^{\frac{L}{4}}\sum_{k=1,4}\frac{\delta\alpha_0^{(k,j)}-\delta\alpha_1^{(k,j)}}{2}g\mu_b\mathbf{B}\cdot\mathbf{d}_k t_k e^{-2\gamma_k t_k}\\ &+\sum_{j=1}^{\frac{L}{4}}\sum_{k=2,3}\frac{\delta\alpha_0^{(k,j)}-\delta\alpha_1^{(k,j)}}{2}g\mu_b\mathbf{B}\cdot\mathbf{d}_k t_k e^{-2\gamma_k t_k}\\ &-\sum_{j=1}^{\frac{L}{4}}\sum_{k=1,4}\frac{\alpha_0^{(k)}-\alpha_1^{(k)}}{2}g\mu_b\mathbf{B}\cdot\mathbf{d}_k t_k e^{-2\gamma_k t_k}(-2\delta\gamma_{k,j}t_k)\\ &+\sum_{j=1}^{\frac{L}{4}}\sum_{k=2,3}\frac{\alpha_0^{(k)}-\alpha_1^{(k)}}{2}g\mu_b\mathbf{B}\cdot\mathbf{d}_k t_k e^{-2\gamma_k t_k}(-2\delta\gamma_{k,j}t_k),\end{aligned}$$

where we use $e^{-2\gamma_{l,j}t_l} = e^{-2\gamma_l t_l}e^{-2\delta\gamma_{l,j}t_l} \simeq e^{-2\gamma_l t_l}(1-2\delta\gamma_{l,j}t_l)$ for $l = 1,2,3,4$. From the central limit theorem, we can show $\delta N_x^{(\mathrm{av})} = O(\sqrt{L})$ while we have $N_x^{(\mathrm{av})} = O(L)$. So we have $\langle\hat{N}_x^{(\mathrm{total})}\rangle \simeq N_x^{(\mathrm{av})}$ for a large L, and so the effect of the inhomogeneous parameters is negligible. Therefore, even for an ensemble of NV centers where each NV center has different decay rate and visibility, we can use our scheme to measure the vector magnetic field, similarly to the case of four NV centers described above.

IV. AC-VECTOR-MAGNETIC-FIELD SENSOR VIA MULTIFREQUENCY CONTROL

Here, we explain how to measure the ac vector magnetic field using our scheme. As an example, we discuss the case of measuring the x component of the ac magnetic fields. We use a similar pulse sequence to that in our dc magnetic field sensing. The only difference from the dc magnetic field sensing is that we apply a π pulse in the middle of the microwave pulse sequence as shown in Fig. 3(b). Similarly to the case of dc magnetic field sensing, we can use a large ensemble

of NV centers for the ac field sensing. However, we start by explaining how our scheme for ac field sensing works if we have four specific NV centers with the NV axis of $\mathbf{d}_1$, $\mathbf{d}_2$, $\mathbf{d}_3$, and $\mathbf{d}_4$. After the green laser irradiation, the state of the photons can be described as follows:

$$\rho_{\rm ac}^{(\rm ph)} = \bigotimes_{l=1}^{4} \rho_{l,\rm ac}^{(\rm ph)}, \tag{29}$$

where

$$\rho_{k,\rm ac}^{(\rm ph)} = \frac{1+e^{-2\gamma_k' t_k}\sin\theta_k^{(\rm ac)}}{2}\rho_{k,0}^{(\rm ph)} + \frac{1-e^{-2\gamma_k' t_k}\sin\theta_k^{(\rm ac)}}{2}\rho_{k,1}^{(\rm ph)}$$

for $k = 2,3$ and

$$\rho_{k,\rm ac}^{(\rm ph)} = \frac{1-e^{-2\gamma_k' t_k}\sin\theta_k^{(\rm ac)}}{2}\rho_{k,0}^{(\rm ph)} + \frac{1+e^{-2\gamma_k' t_k}\sin\theta_k^{(\rm ac)}}{2}\rho_{k,1}^{(\rm ph)}$$

for $k = 1,4$. We can calculate the expected values of the emitted photon from these states as follows:

$$\begin{aligned}\langle \hat{N}_x^{(\rm total)}\rangle &\simeq \left(\sum_{l=1}^{4}\frac{\alpha_0^{(l)}+\alpha_1^{(l)}}{2}\right) \\ &\quad - \sum_{k=1,4}\frac{(\alpha_0^{(k)}-\alpha_1^{(k)})g\mu_b\mathbf{B}_{\rm ac}\cdot\mathbf{d}_k\frac{1+\cos\omega_{\rm ac}t_k-2\cos\frac{\omega_{\rm ac}t_k}{2}}{\omega_{\rm ac}}e^{-2\gamma_k' t_k}}{2} \\ &\quad + \sum_{k=2,3}\frac{(\alpha_0^{(k)}-\alpha_1^{(k)})g\mu_b\mathbf{B}_{\rm ac}\cdot\mathbf{d}_k\frac{1+\cos\omega_{\rm ac}t_k-2\cos\frac{\omega_{\rm ac}t_k}{2}}{\omega_{\rm ac}}e^{-2\gamma_k' t_k}}{2}.\end{aligned}$$

If we have $\alpha_0^{(l)} = \alpha_0$, $\alpha_1^{(l)} = \alpha_1$, $\gamma_l' = \gamma$, and $t_l = t$ for $l = 1,2,3,4$, we obtain

$$\begin{aligned}\langle \hat{N}_x^{(\rm total)}\rangle &\simeq 2(\alpha_0+\alpha_1) \\ &\quad - \frac{2(\alpha_0-\alpha_1)g\mu_b B_x^{(\rm ac)}\left(1+\cos\omega_{\rm ac}t-2\cos\frac{\omega_{\rm ac}t}{2}\right)e^{-2\gamma' t}}{\sqrt{3}\,\omega_{\rm ac}}.\end{aligned}$$

Note that this expectation value only depends on $B_x^{(\rm ac)}$. Therefore, the uncertainty in the estimation of $B_x^{(\rm ac)}$ is given as follows:

$$\begin{aligned}\delta B_x^{(\rm ac)} &= \frac{\sqrt{\langle \delta\hat{N}_x^{(\rm total)}\delta\hat{N}_x^{(\rm total)}\rangle}}{\left|\frac{d\langle \hat{N}_x^{(\rm total)}\rangle}{dB_x^{(\rm ac)}}\right|}\frac{1}{\sqrt{N}} \\ &\simeq \frac{\sqrt{2(\alpha_0+\alpha_1)}}{\frac{2}{\sqrt{3}}|\alpha_0-\alpha_1|g\mu_b\frac{|1+\cos\omega_{\rm ac}t-2\cos\frac{\omega_{\rm ac}t}{2}|}{\omega_{\rm ac}}e^{-2\gamma' t}}\frac{1}{\sqrt{\frac{T}{t}}},\end{aligned}$$

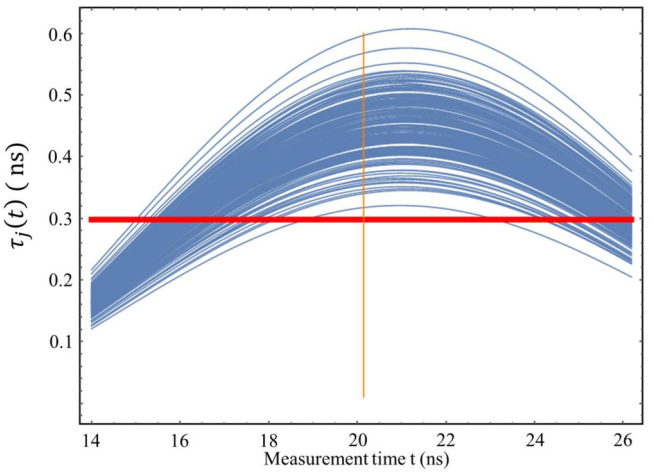

FIG. 6. We plot $\tau_j'(t) = \frac{\alpha_0^{(j)}-\alpha_1^{(j)}}{2}e^{-2\gamma_j' t}\frac{1+\cos(\omega_{\rm ac}t)-2\cos(\frac{\omega_{\rm ac}}{2}t)}{\omega_{\rm ac}}$ $(j = 1,2,\ldots,200)$ against t where we choose $\delta\alpha_j = \alpha_0^{(j)} - \alpha_1^{(j)}$ and γ_j' from the Gaussian distribution. The average of $\delta\alpha_j$ (γ_j') is 0.01 (10^7), and the standard deviation is 0.001 (10^6). In addition, we plot the value of $\frac{\delta\alpha_{\rm min}}{2}e^{-\frac{1}{2}}\frac{1+\cos(\theta_{\rm opt})-2\cos(\frac{\theta_{\rm opt}}{2})}{\omega_{\rm ac}}$ with a horizontal dashed line, and we plot a vertical line at $t = \frac{1}{4\gamma'_{\rm max}}$ where $\delta\alpha_{\rm min} = \min_j[\delta\alpha_j]$, $\gamma'_{\rm max} = \max_j[\gamma_j']$, and $\omega_{\rm ac} = 4\theta_{\rm opt}\gamma'_{\rm max}$. We numerically show that we can satisfy $\tau_j'(t_j) = \frac{\delta\alpha_{\rm min}}{2}e^{-\frac{1}{2}}\frac{1+\cos(\theta_{\rm opt})-2\cos(\frac{\theta_{\rm opt}}{2})}{\omega_{\rm ac}}$ for all j by choosing a certain set of $\{t_j\}_{j=1}^{200}$ where $t_j \leqslant \frac{1}{4\gamma'_{\rm max}}$.

where $N = \frac{T}{t}$ denotes the repetition number of the experiment. By optimizing the parameters, we obtain

$$\delta B_x^{(\rm ac)} \simeq \frac{\sqrt{3}\sqrt{2(\alpha_0+\alpha_1)}}{2e^{-\frac{1}{2}}|\alpha_0-\alpha_1|g\mu_b\frac{|1+\cos\theta_{\rm opt}-2\cos\frac{\theta_{\rm opt}}{2}|}{\theta_{\rm opt}}\sqrt{\frac{1}{4\gamma'}}}\frac{1}{\sqrt{T}}.$$

Because $\alpha_0 \simeq \alpha_1$, we can conclude that the sensitivity of our scheme is approximately four times better than that in the conventional scheme by comparing Eq. (30) with Eq. (18).

Conversely, if the parameters $\alpha_0^{(l)}$, $\alpha_1^{(l)}$, and γ_l' have a dependency on k, we need to choose a suitable set of t_l $(l = 1,2,3,4)$ to compensate such an inhomogeneity. We know that if $(\alpha_0^{(l)} - \alpha_1^{(l)})e^{-2\gamma_l' t_l}\frac{1+\cos\omega_{\rm ac}t_l-2\cos\frac{\omega_{\rm ac}t_l}{2}}{\omega_{\rm ac}}$ does not depend on l, we can estimate the value of $B_x^{(\rm ac)}$ from just $\langle \hat{N}_x^{(\rm total)}\rangle$. We numerically checked whether it is possible to have an equal value of $(\alpha_0^{(l)} - \alpha_1^{(l)})e^{-2\gamma_l' t_l}\frac{1+\cos\omega_{\rm ac}t_l-2\cos\frac{\omega_{\rm ac}t_l}{2}}{\omega_{\rm ac}}$ for all l. In Fig. 6, we randomly picked $\delta\alpha_j = \alpha_0^{(j)} - \alpha_1^{(j)}$ and γ_j' from the Gaussian distribution. We plotted $\tau_j'(t) = \frac{\alpha_0^{(j)}-\alpha_1^{(j)}}{2}e^{-2\gamma_j' t}\frac{1+\cos(\omega_{\rm ac}t)-2\cos(\frac{\omega_{\rm ac}}{2}t)}{\omega_{\rm ac}}$ $(j = 1,2,\ldots,200)$ and the value of $\frac{\delta\alpha_{\rm min}}{2}e^{-\frac{1}{2}}\frac{1+\cos(\theta_{\rm opt})-2\cos(\frac{\theta_{\rm opt}}{2})}{\omega_{\rm ac}}$ where $\delta\alpha_{\rm min} = \min_j[\delta\alpha_j]$, $\gamma'_{\rm max} = \max_j[\gamma_j']$, and $\omega_{\rm ac} = 4\theta_{\rm opt}\gamma'_{\rm max}$. These results show that we can choose t_j to satisfy $\tau_j'(t_j) = \frac{\delta\alpha_{\rm min}}{2}e^{-\frac{1}{2}}\frac{1+\cos(\theta_{\rm opt})-2\cos(\frac{\theta_{\rm opt}}{2})}{\omega_{\rm ac}}$ for all j where $t_j \leqslant \frac{1}{4\gamma'_{\rm max}}$.

We can calculate the expected values of the emitted photons from this state as follows:

$$\left\langle \hat{N}_x^{(\mathrm{total})} \right\rangle \simeq \left(\sum_{l=1}^{4} \frac{\alpha_0^{(l)} + \alpha_1^{(l)}}{2} \right) - \frac{2e^{-\frac{1}{2}} \delta\alpha_{\min} g\mu_b B_x^{(\mathrm{ac})} \left(1 + \cos\theta_{\mathrm{opt}} - 2\cos\frac{\theta_{\mathrm{opt}}}{2}\right)}{\sqrt{3}\omega_{\mathrm{ac}}}, \quad (30)$$

where $\delta\alpha_{\min} = \min_{l=1,2,3,4}[\delta\alpha_l]$, $\gamma'_{\max} = \max_{l=1,2,3,4}[\gamma'_l]$, and $\omega_{\mathrm{ac}} = 4\theta_{\mathrm{opt}}\gamma'_{\max}$. Therefore, the uncertainty is

$$\delta B_x^{(\mathrm{ac})} \simeq \frac{\sqrt{3}\sqrt{\sum_{l=1}^{4} \frac{\alpha_0^{(l)} + \alpha_1^{(l)}}{2}}}{2e^{-\frac{1}{2}} \delta\alpha_{\min} g\mu_b \frac{|1+\cos\theta_{\mathrm{opt}} - 2\cos\frac{\theta_{\mathrm{opt}}}{2}|}{\theta_{\mathrm{opt}}} \sqrt{\frac{1}{4\gamma'_{\max}}}} \frac{1}{\sqrt{T}}.$$

Similarly to the case of dc-vector-magnetic-field sensing, we can achieve nearly the same sensitivity as that in the homogeneous case if the standard deviation of the parameters is around a few % as shown in Fig. 5.

It is worth mentioning that although we have described a scheme to measure the vector of the ac magnetic field by using four NV centers, it is possible to use a large ensemble of NV centers where each NV center has different decay rate. Similarly to the dc magnetic field sensing, we can use a central limit theorem so that the statistical variations can be negligible as long as the number of the NV centers is large.

In conclusion, we proposed a scheme to improve the sensitivity of vector-magnetic-field sensing via multifrequency control. Implementing a Ramsey interference or spin echo experiment for all NV centers with different NV axes using frequency selectivity, we can enhance the signal from the NV centers. We demonstrated that the sensitivity of the vector-magnetic-field sensing becomes approximately four times better than that of the conventional scheme.

ACKNOWLEDGMENTS

We thank Suguru Endo for useful discussion. This work was supported by JSPS KAKENHI Grant No. 15K17732. This work was also supported by MEXT KAKENHI Grants No. 15H05868, No. 15H05870, No. 15H03996, No. 26220602, and No. 26249108. This work was also supported by the Advanced Photon Science Alliance (APSA), JSPS Core-to-Core Program FY2013 Projects No. 2, and Spin-NRJ.

APPENDIX A: TWO-LEVEL SYSTEM APPROXIMATION FOR THE NV CENTER

Although the NV center is a spin-1 system, we can approximate this system as a two-level system by using a frequency selectivity. We will show the details for this approximation. The Hamiltonian of the NV center with an NV axis of $\mathbf{d}_k$ is

$$H_k = \omega_0 \left(\hat{S}_z^{(k)}\right)^2 + g\mu_b \mathbf{B}_{\mathrm{ex}} \cdot \mathbf{d}_k \hat{S}_z^{(k)} + \lambda' \hat{S}_x^{(k)} \cos\omega' t, \quad (A1)$$

where $\hat{S}_x$, $\hat{S}_y$, and $\hat{S}_z$ denote spin-1 operators. It is worth mentioning that although the NV center is affected by a strain, we can remove the effect of the strain from the Hamiltonian by applying external magnetic fields [33,34]. So, in this paper, we do not consider the effect of the strain. By going to a rotating frame with a frequency of $\omega' = \omega_0 + g\mu_b \mathbf{B}_{\mathrm{ex}} \cdot \mathbf{d}_k$, we obtain

$$H_k = (\omega_0 - \omega')\left(\hat{S}_z^{(k)}\right)^2 + g\mu_b \mathbf{B}_{\mathrm{ex}} \cdot \mathbf{d}_k \hat{S}_z^{(k)} + \frac{\lambda'}{\sqrt{2}}(|0\rangle_k\langle 1| + |1\rangle_k\langle 0|),$$

where we use the rotating-wave approximation. Since we consider $|0\rangle_k$ as an initial state, the state of $|-1\rangle_k$ will not be involved in the dynamics by this Hamiltonian, and so we can ignore the state of $|-1\rangle_k$. So we obtain

$$H_k = (\omega_0 - \omega' + g\mu_b \mathbf{B}_{\mathrm{ex}} \cdot \mathbf{d}_k)|1\rangle_k\langle 1| + \frac{\lambda'}{\sqrt{2}}(|0\rangle_k\langle 1| + |1\rangle_k\langle 0|),$$

and we can rewrite this Hamiltonian as follows:

$$H_k = \frac{(\omega_0 - \omega' + g\mu_b \mathbf{B}_{\mathrm{ex}} \cdot \mathbf{d}_k)}{2} \hat{\sigma}_z^{(k)} + \frac{\lambda'}{\sqrt{2}} \hat{\sigma}_x^{(k)},$$

where $\hat{\sigma}_z^{(k)} = |1\rangle_k\langle 1| - |0\rangle_k\langle 0|$ and $\hat{\sigma}_x^{(k)} = |0\rangle_k\langle 1| + |1\rangle_k\langle 0|$. Therefore, we can treat the NV center as a two-level system.

APPENDIX B: THE EFFECT OF THE MICROWAVE PULSES ON THE NV CENTERS

In the main text, we assume the Hamiltonian of the NV center with an axis with $\mathbf{d}_k$ as

$$H_k = \frac{\omega_l}{2} \hat{\sigma}_z^{(k)} + \lambda \hat{\sigma}_x^{(k)} \cos\omega' t, \quad (B1)$$

where the microwave pulses are applied along the x direction on the NV center. However, in our scheme, the microwave field to drive the other NV centers with different axes ($\mathbf{d}_{k'}$ for $k' \neq k$) has parallel and perpendicular components to the axis of $\mathbf{d}_k$. To consider the effect of the microwave pulses to drive the other NV centers, we use the following Hamiltonian:

$$H_k = \frac{\omega_l}{2} \hat{\sigma}_z^{(k)} + \lambda \hat{\sigma}_x^{(k)} \cos\omega' t + \tilde{\lambda}_x \hat{\sigma}_x^{(k)} \cos\tilde{\omega}' t + \tilde{\lambda}_z \hat{\sigma}_z^{(k)} \cos\tilde{\omega}' t, \quad (B2)$$

where λ_x (λ_z) denote the amplitude of the microwave along the x (z) direction to drive the other NV centers, $\omega' = \omega_0 + g\mu_b \mathbf{B}_{\mathrm{ex}} \cdot \mathbf{d}_k$ denotes the frequency of the resonant microwave on the target NV center, $\tilde{\omega}' = \omega' + \delta$ denotes the frequency of the microwave for the other NV centers, and δ denotes the detuning between the NV centers. By going to a rotating frame, we obtain

$$H_k = \frac{\omega_l - \omega'}{2} \hat{\sigma}_z^{(k)} + \lambda \hat{\sigma}_x^{(k)} \frac{1 + e^{2i\omega' t}}{2} + \tilde{\lambda}_x \hat{\sigma}_x^{(k)} \frac{e^{i(\omega' + \tilde{\omega}')t} + e^{i(\omega' - \tilde{\omega}')t}}{2} + \tilde{\lambda}_z \hat{\sigma}_z^{(k)} \cos\tilde{\omega}' t.$$

Importantly, by using a rotating-wave approximation, we obtain a time-independent Hamiltonian

$$H_k \simeq \frac{\omega_l - \omega'}{2} \hat{\sigma}_z^{(k)} + \frac{\lambda}{2} \hat{\sigma}_x^{(k)}, \quad (B3)$$

and so the effect of the microwave to drive other NV centers is negligible. Also, by using a numerical simulation, we have confirmed that the perpendicular component does not affect the dynamics with realistic parameters as shown in Fig. 7.

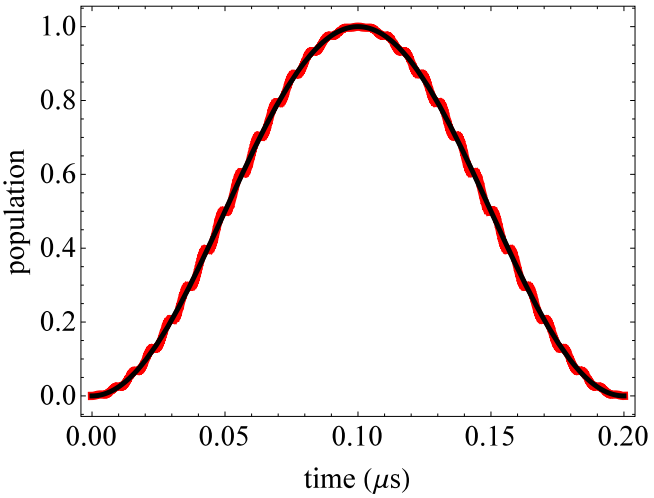

FIG. 7. We plot the population of the NV center ${}_l\langle 1|\rho_k(t)|1\rangle_l$ with the Hamiltonian in Eq. (B2) [Eq. (B3)] by a red (black) line where the initial state is $\rho_l(0) = |0\rangle_l\langle 0|$. The parameters are $\lambda = \tilde{\lambda}_x = \tilde{\lambda}_y = 2\pi \times 5$ MHz, $\omega_l = \omega' = 2\pi \times 3$ GHz, and $\delta = 2\pi \times 150$ MHz. Although we have a small oscillation with the time-dependent Hamiltonian, the dynamics with the time-dependent Hamiltonian is similar to that with the time-independent Hamiltonian. These results show that the rotating-wave approximation is valid in this parameter regime.

APPENDIX C: IMPERFECT SINGLE-QUBIT ROTATIONS

For an ensemble of NV centers, each NV center is affected by slightly different magnetic fields due to the environmental spins, and this induces a finite linewidth in the spectrum [24]. Importantly, due to the inhomogeneous magnetic fields, we cannot apply a perfect $\frac{\pi}{2}$ pulse on the ensemble of the NV centers. However, as we will show below, the effect of the imperfect single-qubit rotation is negligible in our scheme as long as the Rabi frequency is larger than the inhomogeneous linewidth.

We describe the Hamiltonian under the effect of the inhomogeneous magnetic fields. In a rotating frame, we can rewrite this Hamiltonian of the jth NV center ($j = 1,2,\ldots,\frac{L}{4}$) with an NV axis of $\mathbf{d}_k$ as

$$H_{k,x}^{(j)} = \frac{\omega_k^{(j)} - \omega_k'}{2}\hat{\sigma}_z^{(k)} - \frac{\lambda}{2}\hat{\sigma}_x^{(k)},$$
$$H_{k,y}^{(j)} = \frac{\omega_k^{(j)} - \omega_k'}{2}\hat{\sigma}_z^{(k)} - \frac{\lambda}{2}\hat{\sigma}_y^{(k)}, \tag{C1}$$

where $\omega_k^{(j)} = \omega_0 + g\mu_b\mathbf{B}_{\text{total}}^{(j)}\cdot\mathbf{d}_k$, $\mathbf{B}_{\text{total}}^{(j)} = \mathbf{B}_{\text{ex}} + \mathbf{B} + \mathbf{B}^{(j)}$, and $\omega_k' = \omega_0 + g\mu_b\mathbf{B}_{\text{ex}}\cdot\mathbf{d}_k$. Here, $\mathbf{B}_{\text{ex}}$ denotes the applied known magnetic fields, $\mathbf{B}$ denotes the target magnetic fields to be sensed, and $\mathbf{B}^{(j)}$ denotes inhomogeneous magnetic fields on the jth NV center. We can rewrite the Hamiltonian as

$$H_{k,x}^{(j)} = n_j\frac{\lambda}{2}\hat{\sigma}_z^{(k)} - \frac{\lambda}{2}\hat{\sigma}_x^{(k)}, \tag{C2}$$
$$H_{k,y}^{(j)} = n_j\frac{\lambda}{2}\hat{\sigma}_z^{(k)} - \frac{\lambda}{2}\hat{\sigma}_y^{(k)}, \tag{C3}$$

where $n_{k,j} = \frac{g\mu_b\mathbf{B}\cdot\mathbf{d}_k + g\mu_b\mathbf{B}^{(j)}\cdot\mathbf{d}_k}{\lambda}$. Also, we define a Hamiltonian without microwave driving as

$$H_k^{(j)} = n_j\frac{\lambda}{2}\hat{\sigma}_z^{(k)}. \tag{C4}$$

We consider the dynamics of the states of the NV centers with NV axes of $\mathbf{d}_1$ and $\mathbf{d}_4$ when we implement a pulse sequence for our vector-magnetic-field sensor. First, by using green laser irradiation, we prepare a state of $|0\rangle_{k,j}$. Second, by performing the $\frac{\pi}{2}$ pulse by the Hamiltonian $H_{k,y}^{(j)}$, we obtain $e^{-iH_{k,y}^{(j)}\frac{\pi}{2\lambda}}|0\rangle_{k,j}$. Third, we let the state evolve for time $t = \frac{1}{4\gamma}$, and we obtain the state described by a density matrix $\rho_{k,j}(t)$ after the time evolution by solving the master equation

$$\frac{d\rho_{k,j}}{dt} = -i\left[H_k^{(j)},\rho_{k,j}\right] - \gamma\left(\rho_{k,j} - \hat{\sigma}_z^{(k)}\rho_{k,j}\hat{\sigma}_z^{(k)}\right) \tag{C5}$$

for a given initial state of $e^{-iH_{k,y}^{(j)}\frac{\pi}{2\lambda}}|0\rangle_{k,j}$. Here, for simplicity, we consider a homogeneous decay rate γ. Finally, we perform the $\frac{\pi}{2}$ pulse by the Hamiltonian $H_{k,x}^{(j)}$, and obtain $\rho_{k,j}^{(\text{f})} = e^{-iH_{k,y}^{(j)}\frac{\pi}{2\lambda}}\rho_{k,j}(t)e^{iH_{k,y}^{(j)}\frac{\pi}{2\lambda}}$. Since only the diagonal component of this density matrix affects the optical readout, we calculate these as follows:

$${}_{k,j}\langle 0|\rho_{k,j}^{(\text{f})}|0\rangle_{k,j} \simeq \frac{1}{2} + \frac{\lambda n_{k,j}}{8\sqrt{e}\gamma} + O\left(n_{k,j}^3\right),$$
$${}_{k,j}\langle 1|\rho_{k,j}^{(\text{f})}|1\rangle_{k,j} \simeq \frac{1}{2} - \frac{\lambda n_{k,j}}{8\sqrt{e}\gamma} + O\left(n_{k,j}^3\right),$$

where we assume $n_{k,j} \ll 1$ and $\gamma \ll \lambda$. Similarly, we can calculate the states of the NV centers with NV axes of $\mathbf{d}_2$ and $\mathbf{d}_3$. The expected values of the emitted photons from the NV centers after the readout by the green laser is calculated as

$$\left\langle\hat{N}_x^{(\text{total})}\right\rangle \simeq \sum_{j=1}^{\frac{L}{4}} 2(\alpha_0+\alpha_1) - \sum_{j=1}^{\frac{L}{4}}\sum_{k=1,4}\frac{\alpha_0-\alpha_1}{2}n_{k,j}\lambda\frac{1}{4\gamma}e^{-\frac{1}{2}}$$
$$+ \sum_{j=1}^{\frac{L}{4}}\sum_{k=2,3}\frac{\alpha_0-\alpha_1}{2}n_{k,j}\frac{1}{4\gamma}e^{-\frac{1}{2}} + O\left(n_{k,j}^3\right), \tag{C6}$$

where we assume homogeneous photon emission probabilities. Since $\overline{n_k} = \frac{1}{(L/4)}\sum_{j=1}^{\frac{L}{4}} n_{j,k}$ denotes the average value of $\{n_{k,j}\}_{j=1}^{j=\frac{L}{4}}$, we obtain

$$\left\langle\hat{N}_x^{(\text{total})}\right\rangle \simeq \frac{L}{2}(\alpha_0+\alpha_1) - \frac{L}{4}\sum_{k=1,4}\frac{\alpha_0-\alpha_1}{2}\overline{n_k}\lambda\frac{1}{4\gamma}e^{-\frac{1}{2}}$$
$$+ \frac{L}{4}\sum_{k=2,3}\frac{\alpha_0-\alpha_1}{2}\overline{n_k}\frac{1}{4\gamma}e^{-\frac{1}{2}} + O\left(n_{k,j}^3\right)$$
$$\simeq \frac{L}{2}(\alpha_0+\alpha_1) - \frac{L}{4}\sum_{k=1,4}\frac{\alpha_0-\alpha_1}{2}g\mu_b\mathbf{B}\cdot\mathbf{d}_k\lambda\frac{1}{4\gamma}e^{-\frac{1}{2}}$$
$$+ \frac{L}{4}\sum_{k=2,3}\frac{\alpha_0-\alpha_1}{2}g\mu_b\mathbf{B}\cdot\mathbf{d}_k\frac{1}{4\gamma}e^{-\frac{1}{2}} + O(n_{k,j}^3), \tag{C7}$$

where $\overline{n_k} = \frac{1}{\lambda} \cdot \overline{g\mu_b \mathbf{B} \cdot \mathbf{d}_k + g\mu_b \mathbf{B}^{(j)} \cdot \mathbf{d}_k} = \frac{g\mu_b \mathbf{B} \cdot \mathbf{d}_k}{\lambda}$. Therefore, the effect of the inhomogeneous broadening does not appear in the perturbative calculation with $\frac{g\mu_b \mathbf{B} \cdot \mathbf{d}_k + g\mu_b \mathbf{B}^{(j)} \cdot \mathbf{d}_k}{\lambda} \ll 1$, and so we can implement our vector-magnetic-field sensing as long as we strongly drive the NV centers by the microwave pulses.

APPENDIX D: THE EFFECT OF THE STANDARD DEVIATION OF THE PHOTON NUMBER ON THE PRECISION OF OUR MAGNETIC FIELD SENSOR

Here, we show that the sensitivity of our magnetic field sensor does not depend on the standard deviation of the emitted photons but depends on the average number of the photons.

The sensitivity of the field sensing is calculated by the following formula:

$$\delta B = \frac{\sqrt{\langle \delta\hat{N} \delta\hat{N} \rangle}}{\left| \frac{d\langle \hat{N} \rangle}{dB} \right|} \frac{1}{\sqrt{N}}, \tag{D1}$$

where δB denotes the uncertainty of the estimation, $\hat{N} = \hat{a}^\dagger \hat{a}$ denotes the number operator of the emitted photons, $\delta\hat{N} = \hat{N} - \langle \hat{N} \rangle$ denotes the deviation from the average number of the emitted photons, and N denotes the number of the repetition. Since we assume that the collection efficiency of the photon is small, we can approximate the number operator of the photons as $\hat{N} = \sum_{n=0}^{\infty} n |n\rangle_{\rm ph} \langle n| \simeq |1\rangle_{\rm ph} \langle 1|$ where $|n\rangle_{\rm ph}$ denotes the Fock states of the photons. We obtain

$$\begin{aligned} \langle \delta\hat{N} \delta\hat{N} \rangle &= \langle \hat{N}^2 \rangle - \langle \hat{N} \rangle^2 \\ &\simeq \langle \hat{N} \rangle - \langle \hat{N} \rangle^2. \end{aligned} \tag{D2}$$

Therefore, we can rewrite Eq. (D1) as follows:

$$\delta B \simeq \frac{\sqrt{\langle \hat{N} \rangle}}{\left| \frac{d\langle \hat{N} \rangle}{dB} \right|} \frac{1}{\sqrt{N}}, \tag{D3}$$

where we assume $\hat{N} \ll 1$. This shows that the sensitivity of our magnetic field sensor simply depends on the average number of emitted photons and the repetition number.

[1] J. Simon, Adv. Phys. **48**, 449 (1999).
[2] A. Chang, H. Hallen, L. Harriott, H. Hess, H. Kao, J. Kwo, R. Miller, R. Wolfe, J. Van der Ziel, and T. Chang, Appl. Phys. Lett. **61**, 1974 (1992).
[3] M. Poggio and C. Degen, Nanotechnology **21**, 342001 (2010).
[4] J. Maze, P. Stanwix, J. Hodges, S. Hong, J. Taylor, P. Cappellaro, L. Jiang, M. Dutt, E. Togan, A. Zibrov, *et al.*, Nature (London) **455**, 644 (2008).
[5] J. Taylor, P. Cappellaro, L. Childress, L. Jiang, D. Budker, P. Hemmer, A. Yacoby, R. Walsworth, and M. Lukin, Nat. Phys. **4**, 810 (2008).
[6] G. Balasubramanian, I. Chan, R. Kolesov, M. Al-Hmoud, J. Tisler, C. Shin, C. Kim, A. Wojcik, P. Hemmer, A. Krueger *et al.*, Nature (London) **455**, 648 (2008).
[7] M. Schaffry, E. M. Gauger, J. J. L. Morton, and S. C. Benjamin, Phys. Rev. Lett. **107**, 207210 (2011).
[8] G. Davies, *Properties and Growth of Diamond* (INSPEC/IEE, London, 1994).
[9] A. Gruber, A. Dräbenstedt, C. Tietz, L. Fleury, J. Wrachtrup, and C. Von Borczyskowski, Science **276**, 2012 (1997).
[10] F. Jelezko, I. Popa, A. Gruber, C. Tietz, J. Wrachtrup, A. Nizovtsev, and S. Kilin, Appl. Phys. Lett. **81**, 2160 (2002).
[11] F. Jelezko, T. Gaebel, I. Popa, A. Gruber, and J. Wrachtrup, Phys. Rev. Lett **92**, 076401 (2004).
[12] G. Balasubramanian, P. Neumann, D. Twitchen, M. Markham, R. Kolesov, N. Mizuochi, J. Isoya, J. Achard, J. Beck, J. Tissler, *et al.*, Nat. Mater. **8**, 383 (2009).
[13] N. Mizuochi, P. Neumann, F. Rempp, J. Beck, V. Jacques, P. Siyushev, K. Nakamura, D. Twitchen, H. Watanabe, S. Yamasaki, *et al.*, Phys. Rev. B **80**, 041201 (2009).
[14] N. Bar-Gill, L. M. Pham, A. Jarmola, D. Budker, and R. L. Walsworth, Nat. Commun. **4**, 1743 (2013).
[15] R. Schirhagl, K. Chang, M. Loretz, and C. L. Degen, Annu. Rev. Phys. Chem. **65**, 83 (2014).
[16] B. Maertz, A. Wijnheijmer, G. Fuchs, M. Nowakowski, and D. Awschalom, Appl. Phys. Lett. **96**, 092504 (2010).
[17] S. Steinert, F. Dolde, P. Neumann, A. Aird, B. Naydenov, G. Balasubramanian, F. Jelezko, and J. Wrachtrup, Rev. Sci. Instrum. **81**, 043705 (2010).
[18] L. M. Pham, D. Le Sage, P. L. Stanwix, T. K. Yeung, D. Glenn, A. Trifonov, P. Cappellaro, P. Hemmer, M. D. Lukin, H. Park, *et al.*, New J. Phys. **13**, 045021 (2011).
[19] J. Tetienne, L. Rondin, P. Spinicelli, M. Chipaux, T. Debuisschert, J. Roch, and V. Jacques, New J. Phys. **14**, 103033 (2012).
[20] A. K. Dmitriev and A. K. Vershovskii, J. Opt. Soc. Am. B **33**, B1 (2016).
[21] K. Sasaki, Y. Monnai, S. Saijo, R. Fujita, H. Watanabe, J. Ishi-Hayase, K. M. Itoh, and E. Abe, Rev. Sci. Instrum. **87**, 053904 (2016).
[22] D. Le Sage, K. Arai, D. Glenn, S. DeVience, L. Pham, L. Rahn-Lee, M. Lukin, A. Yacoby, A. Komeili, and R. Walsworth, Nature (London) **496**, 486 (2013).
[23] A. Nowodzinski, M. Chipaux, L. Toraille, V. Jacques, J.-F. Roch, and T. Debuisschert, Microelectron. Reliab. **55**, 1549 (2015).
[24] V. Acosta, E. Bauch, M. Ledbetter, C. Santori, K.-M. Fu, P. Barclay, R. Beausoleil, H. Linget, J. Roch, F. Treussart, *et al.*, Phys. Rev. B **80**, 115202 (2009).
[25] J. Michl, T. Teraji, S. Zaiser, I. Jakobi, G. Waldherr, F. Dolde, P. Neumann, M. W. Doherty, N. B. Manson, J. Isoya, *et al.*, Appl. Phys. Lett. **104**, 102407 (2014).
[26] M. Lesik, J.-P. Tetienne, A. Tallaire, J. Achard, V. Mille, A. Gicquel, J.-F. Roch, and V. Jacques, Appl. Phys. Lett. **104**, 113107 (2014).
[27] T. Fukui, Y. Doi, T. Miyazaki, Y. Miyamoto, H. Kato, T. Matsumoto, T. Makino, S. Yamasaki, R. Morimoto, N. Tokuda, *et al.*, Appl. Phys. Express **7**, 055201 (2014).

[28] M. Geiselmann, M. L. Juan, J. Renger, J. M. Say, L. J. Brown, F. J. G. De Abajo, F. Koppens, and R. Quidant, Nat. Nanotechnol. **8**, 175 (2013).
[29] R. Amsüss, C. H. Koller, T. Nöbauer, S. Putz, S. Rotter, K. Sandner, S. Schneider, M. Schramböck, G. Steinhauser, H. Ritsch, *et al.*, Phys. Rev. Lett. **107**, 060502 (2011).
[30] H. Mamin, M. Kim, M. Sherwood, C. Rettner, K. Ohno, D. Awschalom, and D. Rugar, Science **339**, 557 (2013).
[31] J. Clarke and F. K. Wilhelm, Nature (London) **453**, 1031 (2007).
[32] F. Yoshihara, Y. Nakamura, F. Yan, S. Gustavsson, J. Bylander, W. D. Oliver, and J. S. Tsai, Phys. Rev. B **89**, 020503 (2014).
[33] Y. Matsuzaki, X. Zhu, K. Kakuyanagi, H. Toida, T. Shimooka, N. Mizuochi, K. Nemoto, K. Semba, W. Munro, H. Yamaguchi, *et al.*, Phys. Rev. A **91**, 042329 (2015).
[34] D. Budker and D. F. J. Kimball, *Optical Magnetometry* (Cambridge University Press, Cambridge, 2013).